

Correlated enhancements in $D_s \rightarrow \ell\nu$, $(g-2)$ of muon, and lepton flavor violating τ decays with two R -parity violating couplings

Gautam Bhattacharyya¹, Kalyan Brata Chatterjee¹, and Soumitra Nandi²

¹⁾ Saha Institute of Nuclear Physics, 1/AF Bidhan Nagar, Kolkata 700064, India

²⁾ Dipartimento di Fisica Teorica, Univ. di Torino and INFN, Sezione di Torino, I-10125 Torino, Italy

Abstract

With just two R -parity violating couplings, λ'_{223} and λ'_{323} , we correlate several channels, namely, $D_s \rightarrow \ell\nu$ ($\ell = \mu, \tau$), $(g-2)_\mu$, and some lepton flavor violating τ decays. For $\lambda'_{223} = \lambda'_{323} \sim 0.3$ and for a common superpartner mass of 300 GeV, which explain the recently observed excesses in the above D_s decay channels, we predict the following R -parity violating contributions: $\text{Br}(\tau \rightarrow \mu\gamma) \sim 4.5 \cdot 10^{-8}$, $\text{Br}(\tau \rightarrow \mu\mu\mu) \sim 1.2 \cdot 10^{-8}$, $\text{Br}(\tau \rightarrow \mu\eta/\eta') \sim 4 \cdot 10^{-10}$, and $(g_\mu - 2)/2 \sim 4 \cdot 10^{-11}$. We exhibit our results through observable versus observable correlation plots.

PACS Nos: 12.60.Jv, 13.35.Dx

Key Words: R -parity violation, Lepton flavor violation

1 Motivation

While all attention is now focused on the Large Hadron Collider (LHC) as a possible *gold mine* of physics beyond the standard model (SM), one should not lose sight of other territories rich with new physics, e.g., lepton flavor violating (LFV) rare decays, which could provide complementary information. Ever since neutrino flavor mixing was established, interests for observing flavor violation in charged lepton decays have boomed. While in the neutrino sector flavor violation could be rather large (maximal between ν_μ and ν_τ), in the charged lepton decays there is no sign of flavor violation as yet. The SM contributions to charged LFV decays are quite small, orders of magnitude below the current experimental sensitivity, due to the smallness of neutrino mass. Hence, any observation of LFV processes in the charged lepton sector, which are being probed with ever increasing sensitivity, would unambiguously point to non-standard interactions. Indeed, such indirect observations taken in isolation may not imply much on the exact nature of new physics. But a study of possible correlations of its effects on different independently measured charged LFV observables might provide a powerful cross-check and lead to identification of new physics through LHC/LFV synergy. In this paper, we consider R -parity violating (RPV) supersymmetry [1] and perform a correlation analysis of its numerical impact on different LFV τ decays. We also study at tandem the RPV contribution to $(g-2)_\mu$, an observable which continues to provide a 3σ room for new physics despite significantly improved theoretical and experimental accuracies.

R -parity is a discrete symmetry, which is defined as $R = (-1)^{3B+L+2S}$, where B , L , and S are the baryon number, lepton number and spin of a particle, respectively. R is 1 for all SM particles and -1 for their superpartners. The usual assumption of B and L conservation in supersymmetric models are not supported by any deep underlying principle. The L -violating λ' -type superpotential is written as $\mathcal{W} = \lambda'_{ijk} L_i Q_j D_k^c$, where L_i stands for SU(2) doublet lepton superfields, Q_i for SU(2) doublet quark superfields, D_i^c for SU(2) singlet down-type quark superfields, and $\{i, j, k\}$ are generation indices. There are 27 such λ' couplings, on each of which and also on many of their combinations exist strong constraints [2, 3]. We select *only two* of them, namely λ'_{223} and λ'_{323} , and consider only them to be large and the rest to be either vanishing or negligibly small.

Why λ'_{223} and λ'_{323} ? It has been observed that these two couplings (each with a magnitude of ~ 0.5 and for superparticle masses around 300 GeV) can justify the recently observed large $D_s \rightarrow \ell\nu$ ($\ell = \mu, \tau$) branching ratios that the SM cannot

explain [4]. On top of that, if we turn on even a small $\lambda'_{212} (\sim 0.001)$, then together with $\lambda'_{223} (\sim 0.5)$, one can *also* explain the large phase in $B_s - \bar{B}_s$ mixing [4, 5]. Turning our attention to the neutrino sector, we recall that generation of neutrino masses and mixing by λ' -type couplings usually require a specific combination of indices, namely, the $\lambda'_{ijk} \lambda'_{i'kj}$ product couplings [6]. But if we take λ'_{223} and λ'_{323} (together with λ'_{113}) as the only non-vanishing and large RPV couplings, a phenomenologically acceptable pattern of neutrino masses and mixing emerge at two-loop level [7]. To sum up, we consider four non-vanishing RPV couplings: two of them λ'_{223} and λ'_{323} large (~ 0.5) and relevant for the present analysis, the other two $\lambda'_{212} \sim 0.001$ and $\lambda'_{113} \lesssim 0.1$ (from charged-current universality [2]) not to be used in the present analysis but implicitly present to justify our choices of λ'_{223} and λ'_{323} through the correlated phenomena mentioned above. Now, motivated by the observation of maximal mixing between ν_μ and ν_τ , we make a further assumption $\lambda'_{223} = \lambda'_{323}$. Keeping all these in mind, we outline our agenda as follows: consider λ'_{223} and λ'_{323} as the only two *relevant* RPV couplings (the other two, viz. λ'_{212} and λ'_{113} , optional and small), assume them to be real, set their magnitudes equal and just enough to explain the $D_s \rightarrow \ell\nu$ anomaly, predict its effect on $(g-2)_\mu$, and estimate its numerical impact on different LFV τ decays ($\tau \rightarrow \mu\mu\mu$, $\tau \rightarrow \mu\gamma$, $\tau \rightarrow \mu\eta$, $\tau \rightarrow \mu\eta'$). For simplicity, we assume all squark and slepton masses to be degenerate, and denote the common mass by \tilde{m} . We derive various one-loop effective flavor violating vertices, which we have often referred to as *form-factors*. We display their exact as well as approximate expressions. While for numerical plots we use the exact formulae, the approximate expressions serve to provide an intuitive feel of the numerical impact.

2 $D_s \rightarrow \ell\nu$ and the f_{D_s} anomaly

The branching fraction of the leptonic decay $D_s \rightarrow \ell\nu$ ($\ell = \mu, \tau$) is given by

$$\text{Br}(D_s \rightarrow \ell\nu) = \frac{m_{D_s}}{8\pi} \tau_{D_s} f_{D_s}^2 G_F^2 m_\ell^2 |V_{cs}|^2 \left(1 - \frac{m_\ell^2}{m_{D_s}^2}\right)^2, \quad (1)$$

where τ_{D_s} is the lifetime of D_s . The decay constant is defined as $\langle 0 | \bar{s}\gamma_\mu\gamma_5 c | D_s \rangle = i f_{D_s} p_\mu$, where p_μ is the momentum of D_s . The branching ratio has a helicity suppression factor characterized by m_ℓ^2 on account of a spin-zero particle decaying into two spin-half particles. Monte-Carlo simulations of QCD on lattice predict $f_{D_s} = 241 \pm 3$ MeV [8]. The experimental average is somewhat higher: $f_{D_s} = 277 \pm 9$ MeV [9–11]. The enhancements are $(13 \pm 6)\%$ in the muon channel, $(18 \pm 8)\%$ in the tau channel, and $(15 \pm 5)\%$ on average. On the other hand, the lattice estimate and the experimentally obtained value for f_D seem to be in perfect agreement around 206 MeV [8]. The latter suggests that the discrepancy in f_{D_s} may very well be influenced by new physics contributing in a *flavor specific way* to D_s decay. Note that $D_s \rightarrow \ell\nu$ in the SM proceeds at tree level and it is Cabibbo-allowed. Hence, loop suppressed new physics is an unlikely candidate to account for the discrepancy. Leptoquark or charged Higgs interactions have been advocated in this context as they provide new tree amplitudes for the above decay [12]. Our candidate is supersymmetric RPV interaction and our chosen couplings, λ'_{223} and λ'_{323} , contribute to $D_s \rightarrow \ell\nu_\ell$ ($\ell = \mu, \tau$) via \tilde{b}_R -exchanged *tree* graphs [4]. The net contribution to the $D_s \rightarrow \mu\nu$ channel can be obtained by replacing $G_F^2 |V_{cs}|^2$ in Eq. (1) by

$$\left| G_F V_{cs}^* + \frac{\lambda'_{223}}{4\sqrt{2}\tilde{m}^2} \right|^2 + \left| \frac{\lambda'_{223}\lambda'_{323}}{4\sqrt{2}\tilde{m}^2} \right|^2. \quad (2)$$

For $D_s \rightarrow \tau\nu$, we must do the replacements $\lambda'_{223} \leftrightarrow \lambda'_{323}$ in Eq. (2).

3 Anomalous magnetic moment of the muon

The effective vertex of photon with any charged fermion is given by

$$\bar{u}(p') \Gamma_\mu u(p) = \bar{u}(p') \left[\gamma_\mu F_1(q^2) + \frac{i\sigma_{\mu\nu} q^\nu}{2m_f} F_2(q^2) + \dots \right] u(p). \quad (3)$$

The muon magnetic moment for $f = \mu$ is given by $\vec{\mu} = g_\mu \frac{e}{2m_\mu} \vec{s}$. At tree level, $F_1(0) = 1$ and $F_2(0) = 0$. Quantum correction yields $a_\mu \equiv F_2(0) \neq 0$, while $F_1(0)$ remains unity at all order due to charge conservation. Since $g_\mu \equiv$

$2(F_1(0) + F_2(0))$, it follows that $a_\mu \equiv (g_\mu - 2)/2$. As per current estimation [13], the room for new physics is given by

$$a_\mu^{\text{new}} = a_\mu^{\text{exp}} - a_\mu^{\text{SM}} = (24.6 \pm 8.0) \cdot 10^{-10}. \quad (4)$$

The coupling λ'_{223} induces a contribution to a_μ , which proceeds through the diagrams in Fig. 1. The quarks and squarks

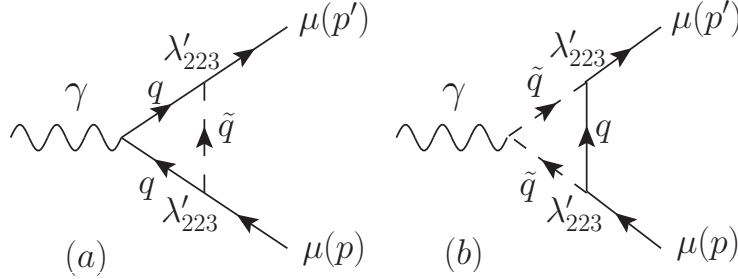


Figure 1: λ'_{223} -induced graphs contributing to $(g - 2)_\mu$. Here, $(q, \tilde{q}) \equiv (c^c, \tilde{b}_R)$ and (b, \tilde{c}_L^*) .

inside the loop have been labeled by generic symbols q and \tilde{q} respectively, which can take two sets: $(q = c^c, \tilde{q} = \tilde{b}_R)$ and $(q = b, \tilde{q} = \tilde{c}_L^*)$. The loop integrals would depend on $r_c \equiv m_c^2/m_{\tilde{b}_R}^2$ and $r_b \equiv m_b^2/m_{\tilde{c}_L}^2$. As mentioned earlier and assumed throughout our analysis, $m_{\tilde{b}_R} = m_{\tilde{c}_L} = \tilde{m}$. We obtain

$$\begin{aligned} a_\mu^{(\lambda')} &= 3 \frac{|\lambda'_{223}|^2 m_\mu^2}{16\pi^2 \tilde{m}^2} [\{Q_c (\xi_1(r_c) - \xi_2(r_c)) + Q_b (\bar{\xi}_1(r_c) - \bar{\xi}_2(r_c))\} \\ &- \{Q_b (\xi_1(r_b) - \xi_2(r_b)) + Q_c (\bar{\xi}_1(r_b) - \bar{\xi}_2(r_b))\}] \simeq 3 \frac{|\lambda'_{223}|^2 m_\mu^2}{16\pi^2 \tilde{m}^2} \left(\frac{1}{6}\right). \end{aligned} \quad (5)$$

The ξ -functions used throughout our analysis are given by

$$\begin{aligned} \xi_n(r) &= \int_0^1 \frac{z^{n+1} dz}{1 + (r-1)z} = \frac{-1}{(1-r)^{n+2}} \left[\ln r + \sum_{k=1}^{n+1} (-1)^k \binom{n+1}{k} \frac{r^k - 1}{k} \right] \\ \bar{\xi}_n(r) &= \frac{1}{r} \xi_n\left(\frac{1}{r}\right). \end{aligned} \quad (6)$$

4 $\tau^- \rightarrow \mu^- \mu^- \mu^+$ decay

The decay $\tau \rightarrow \mu^- \mu^+ \mu^-$ proceeds through photon and Z penguins (Fig. 2) and box graph (Fig. 3). We consider each of them below. Here flavor violation is induced by λ'_{223} and λ'_{323} via loops with quarks and squarks in internal lines.

4.1 Photon penguin

The amplitude of the photon exchanged diagrams for $\tau^- \rightarrow \mu^- \mu^- \mu^+$ decay can be written as

$$M_\gamma = \bar{u}_\mu(p_1) [A_L q^2 \gamma_\mu P_L + i A_R m_\tau \sigma_{\mu\nu} q^\nu P_R] u_\tau(p) \frac{e^2}{q^2} \bar{u}_\mu(p_2) \gamma^\mu v_\mu(p_3) - (p_1 \leftrightarrow p_2), \quad (7)$$

where q is the photon momentum. The form-factors A_L and A_R are induced by the flavor-changing $\lambda'_{223} \lambda'_{323}$ couplings. Each penguin diagram will have a quark (q) and a squark (\tilde{q}) inside the loop. There are two such sets: $(q = c^c, \tilde{q} = \tilde{b}_R)$

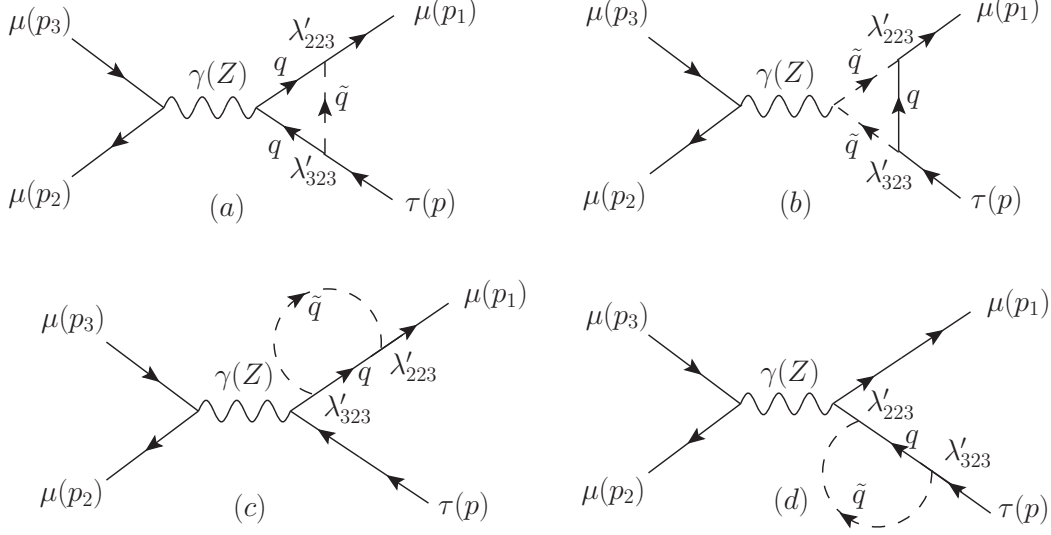


Figure 2: $\lambda_{223}^* \lambda'_{323}$ -induced photon and Z -boson mediated penguins for $\tau^- \rightarrow \mu^- \mu^- \mu^+$. Here, $(q, \tilde{q}) \equiv (c^c, \tilde{b}_R)$ and (b, \tilde{c}_L^*) .

and $(q = b, \tilde{q} = \tilde{c}_L^*)$. We obtain

$$\begin{aligned}
A_L &= \frac{3\lambda_{223}^* \lambda'_{323}}{16\pi^2} \left(\frac{-2}{9\tilde{m}^2} \right) \left[\xi_2(r_c) + \frac{1}{2}\xi_2(r_b) + \frac{1}{4}\bar{\xi}_2(r_c) + \frac{1}{2}\bar{\xi}_2(r_b) \right] \\
&\simeq \frac{3\lambda_{223}^* \lambda'_{323}}{16\pi^2} \left(\frac{1}{9\tilde{m}^2} \right) \left[5 + 4 \ln \left(\frac{m_c}{\tilde{m}} \right) + 2 \ln \left(\frac{m_b}{\tilde{m}} \right) \right].
\end{aligned} \tag{8}$$

The magnetic form-factor is given by

$$\begin{aligned}
A_R &= 3 \frac{\lambda_{223}^* \lambda'_{323}}{32\pi^2 \tilde{m}^2} \left[\{Q_c (\xi_1(r_c) - \xi_2(r_c)) + Q_b (\bar{\xi}_1(r_c) - \bar{\xi}_2(r_c))\} \right. \\
&\quad \left. - \{Q_b (\xi_1(r_b) - \xi_2(r_b)) + Q_c (\bar{\xi}_1(r_b) - \bar{\xi}_2(r_b))\} \right] \simeq 3 \frac{\lambda_{223}^* \lambda'_{323}}{32\pi^2 \tilde{m}^2} \left(\frac{1}{6} \right).
\end{aligned} \tag{9}$$

4.2 Z -boson penguin

The Z -mediated penguin amplitude for the process $\tau^- \rightarrow \mu^- \mu^- \mu^+$ is given by

$$M_Z = \bar{u}_\mu(p_1) [F_L \gamma_\mu P_L] u_\tau(p) \frac{1}{M_Z^2} \bar{u}_\mu(p_2) [\gamma^\mu (a_L^c P_L + a_R^c P_R) v_\mu(p_3)] - (p_1 \leftrightarrow p_2). \tag{10}$$

The Z boson couplings with the left- and right-chiral fermions are given by

$$a_L^f = \frac{g}{\cos \theta_W} (t_3^f - Q_f \sin^2 \theta_W), \quad a_R^f = \frac{g}{\cos \theta_W} (-Q_f \sin^2 \theta_W). \tag{11}$$

The $\lambda_{223}^* \lambda'_{323}$ -induced contribution to the form-factor F_L proceeds through two sets of penguins: $(q = c^c, \tilde{q} = \tilde{b}_R)$ and $(q = b, \tilde{q} = \tilde{c}_L^*)$, yielding

$$F_L = \frac{g}{\cos \theta_W} \left(\frac{3\lambda_{223}^* \lambda'_{323}}{32\pi^2} \right) [r_c \xi_0(r_c) - r_b \xi_0(r_b)] \simeq \frac{g}{\cos \theta_W} \left(\frac{3\lambda_{223}^* \lambda'_{323}}{32\pi^2} \right) \left[\frac{m_b^2}{\tilde{m}^2} \left(1 + 2 \ln \frac{m_b}{\tilde{m}} \right) \right]. \tag{12}$$

4.3 Box contribution

The λ'_{223} and λ'_{323} couplings also induce a box graph for $\tau^- \rightarrow \mu^- \mu^- \mu^+$ with internal quark and squark lines. Again, two sets of box diagrams contribute ($q = c^c, \tilde{q} = \tilde{b}_R$) and ($q = b, \tilde{q} = \tilde{c}_L^*$). The amplitude is given by

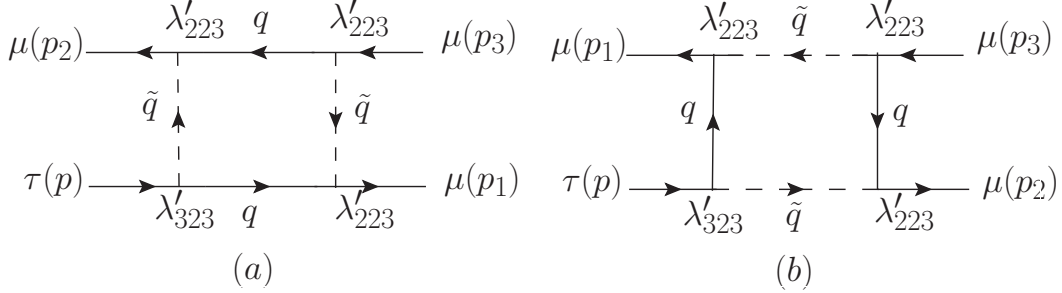


Figure 3: Box graphs for $\tau^- \rightarrow \mu^- \mu^- \mu^+$. Here, $(q, \tilde{q}) \equiv (c^c, \tilde{b}_R)$ and (b, \tilde{c}_L^*) .

$$M_{\text{box}} = e^2 B_L [\bar{u}_\mu(p_1) \gamma^\mu P_L u_\tau(p)] [\bar{u}_\mu(p_2) \gamma_\mu P_L v_\mu(p_3)] - (p_1 \leftrightarrow p_2). \quad (13)$$

For the sake of convenience, we normalize B_L with a prefactor e^2 , though no gauge interaction is actually involved:

$$e^2 B_L = \frac{3\lambda_{223}^{*2} \lambda'_{223} \lambda'_{323}}{64\pi^2 \tilde{m}^2} [f(r_c) + f(r_b)], \quad \text{where } f(r) = \frac{1 - r^2 + 2r \ln(r)}{(1 - r)^3}. \quad (14)$$

4.4 The branching ratio

The total decay amplitude of this process is the sum of the penguin and box contributions, given by $M_{\text{tot}} = M_\gamma + M_Z + M_{\text{box}}$. The branching ratio of $\tau^- \rightarrow \mu^- \mu^- \mu^+$ is given in terms of the different form-factors [14]:

$$\begin{aligned} \text{Br}(\tau^- \rightarrow \mu^- \mu^- \mu^+) &= \frac{e^4 m_\tau^5}{512\pi^3 \Gamma_\tau} \left[A_L^2 - 4A_L A_R + A_R^2 \left(\frac{16}{3} \ln \frac{m_\tau}{m_\mu} - \frac{22}{3} \right) + \frac{1}{6} B_L^2 + \frac{2}{3} A_L B_L - \frac{4}{3} A_R B_L \right. \\ &\quad \left. + \frac{1}{3} (2F_{LL}^2 + F_{LR}^2 + 2B_L F_{LL} + 4A_L F_{LL} + 2A_L F_{LR} - 8A_R F_{LL} - 4A_R F_{LR}) \right], \quad (15) \end{aligned}$$

where Γ_τ is the total decay width of τ . Our form-factors $(A_L, A_R, B_L, F_{LL}, F_{LR})$ are all real. The expressions of F_{LL} and F_{LR} are given by,

$$F_{LL} = \frac{F_L a_L^\ell}{g^2 \sin^2 \theta_W M_Z^2}, \quad F_{LR} = \frac{F_L a_R^\ell}{g^2 \sin^2 \theta_W M_Z^2}. \quad (16)$$

5 Radiative decay $\tau \rightarrow \mu \gamma$

We have shown in Fig. 4 how λ'_{223} together with λ'_{323} drive the magnetic transition $\tau \rightarrow \mu \gamma$. The amplitude for this transition is given by

$$M(\tau \rightarrow \mu \gamma) = A_R m_\tau \bar{u}_\mu(p') (i\sigma_{\mu\nu} q^\nu P_R) u_\tau(p) \epsilon^{\mu*}, \quad (17)$$

where ϵ^μ is the photon polarization. The expression for A_R can be found in Eq. (9). In the amplitude we have neglected a similar term proportional to m_μ . The branching ratio for this radiative decay mode is given by (neglecting any m_μ -dependent term)

$$\text{Br}(\tau^- \rightarrow \mu^- \gamma) = \frac{e^2}{16\pi \Gamma_\tau} m_\tau^5 A_R^2. \quad (18)$$

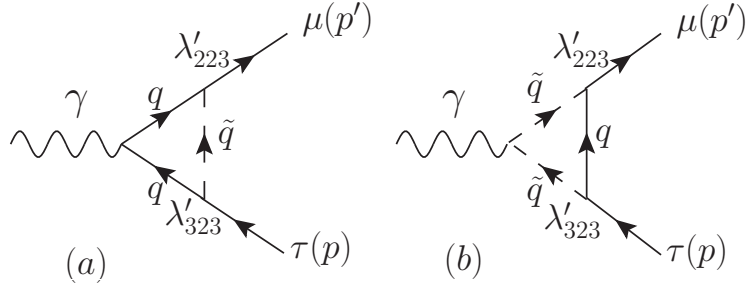


Figure 4: $\lambda'_{223}\lambda'_{323}$ -induced magnetic transition $\tau \rightarrow \mu\gamma$. Here, $(q, \tilde{q}) \equiv (c^c, \tilde{b}_R)$ and (b, \tilde{c}_L^*) .

6 Semileptonic lepton flavor violating τ decay : $\tau \rightarrow \mu\eta(\eta')$

The semileptonic decay $\tau \rightarrow \mu P$ with $P = \eta(\eta')$ decay is mediated by a Z -penguin and a box graph, as shown in Figs. (5a) and (5b), respectively. Photon penguin cannot contribute as it cannot provide the axial current for the quarks to condense to a meson.

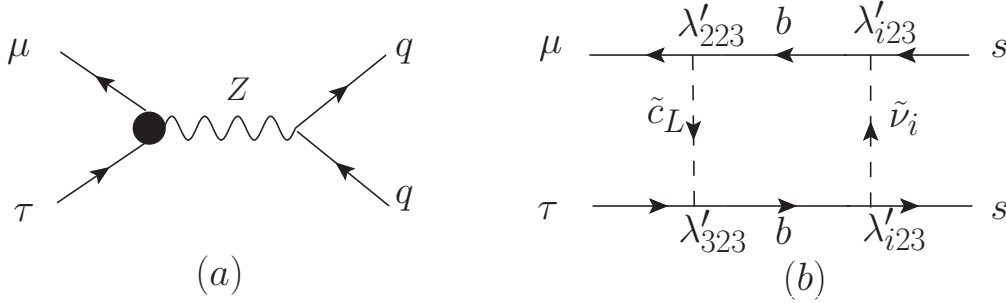


Figure 5: The penguin and box amplitudes for $\tau \rightarrow \mu P$, where $P = \eta, \eta'$. The quark level diagrams are shown, which proceed through (a) Z penguin, and (b) box graph. The blob in (a) is a symbolic representation of lepton flavor violating vertex as in Fig. 2. In (a), we take $q = u, d, s$, all of which contribute to the formation of η and η' . In (b), the specific indices of λ' couplings ensure only $s\bar{s}$ final state is produced. The index i of λ'_{i23} takes two values: $i = 2, 3$. There is another box diagram, not drawn above, where both the internal scalars are \tilde{b}_R and the internal fermions are c and ν_i .

The Z -boson mediated penguin amplitude for $\tau \rightarrow \mu q\bar{q}$ is given by

$$M_Z(\tau \rightarrow \mu q\bar{q}) = \bar{u}_\mu [\gamma_\mu F_L P_L] u_\tau \frac{1}{M_Z^2} \bar{u}_q [\gamma^\mu (a_L^q P_L + a_R^q P_R)] v_q, \quad (19)$$

where a_L^q and a_R^q are given in Eq. (11). The relevant q for the formation of η and η' are u, d and s . The form factor F_L is already given in Eq. (12).

The couplings λ'_{223} and λ'_{323} also induce $\tau \rightarrow \mu q\bar{q}$ through box graphs. Because of the specific λ' -indices, q can only be s . The box graph contains two fermion lines and two scalar lines. There are two types of box diagrams: (i) the fermions are the same (b quark), but the scalars are different (\tilde{c}_L and $\tilde{\nu}_{\mu L}/\tilde{\nu}_{\tau L}$); (ii) the scalars are same (\tilde{b}_R), but the fermions are different (c and ν_μ/ν_τ). The sum of box amplitudes is given by,

$$M_{\text{box}}(\tau \rightarrow \mu s\bar{s}) = D_L [\bar{u}_\mu \gamma^\mu P_L u_\tau] [\bar{u}_s \gamma_\mu P_L v_s]. \quad (20)$$

The form-factor D_L is given by

$$D_L = \frac{3}{64\pi^2\tilde{m}^2} \sum_{i=2,3} \lambda'_{323}\lambda'_{223*} |\lambda'_{i23}|^2 [f(r_b) + f'(r_c)] \simeq \frac{3}{32\pi^2\tilde{m}^2} \sum_{i=2,3} \lambda'_{323}\lambda'_{223*} |\lambda'_{i23}|^2, \quad (21)$$

where $f(r)$ has already been expressed in Eq. (14), while $f'(r)$ is given by

$$f'(r) = \frac{1-r+r\ln(r)}{(1-r)^2}. \quad (22)$$

Using Eqs. (19-22) we obtain the branching ratio,

$$\text{Br}(\tau \rightarrow \mu P) \simeq \frac{(m_\tau^2 - m_P^2)^2}{16\pi m_\tau \Gamma_\tau} \left(\left| \frac{D_L}{2} + \frac{g}{2\cos\theta_W} t_3^s \frac{F_L}{M_Z^2} \right|^2 f_P^{s2} + 2 \left| \frac{g}{2\cos\theta_W} t_3^{u/d} \frac{F_L}{M_Z^2} \right|^2 f_P^{u2} \right). \quad (23)$$

The decay constants involving η and η' are given by

$$\begin{aligned} f_\eta^u = f_\eta^d &= \frac{1}{\sqrt{6}} f_8 \cos\theta_8 - \frac{1}{\sqrt{3}} f_0 \sin\theta_0, & f_{\eta'}^u = f_{\eta'}^d &= \frac{1}{\sqrt{6}} f_8 \sin\theta_8 + \frac{1}{\sqrt{3}} f_0 \cos\theta_0, \\ f_\eta^s &= -\frac{2}{\sqrt{6}} f_8 \cos\theta_8 - \frac{1}{\sqrt{3}} f_0 \sin\theta_0, & f_{\eta'}^s &= -\frac{2}{\sqrt{6}} f_8 \sin\theta_8 + \frac{1}{\sqrt{3}} f_0 \cos\theta_0. \end{aligned} \quad (24)$$

The numerical values of the involved parameters are given by [9, 15];

$$f_8 = 168 \text{ MeV}, \quad f_0 = 157 \text{ MeV}, \quad \theta_8 = -22.2^\circ, \quad \theta_0 = -9.1^\circ, \quad m_\eta (m_{\eta'}) = 547.8 (957.7) \text{ MeV}. \quad (25)$$

7 Results

In Table 1 we have displayed the present experimental status of different branching ratios of our concern.

Decay modes	Branching fractions
$D_s^+ \rightarrow \mu^+ \nu_\mu$	$(6.3 \pm 0.5) \times 10^{-3}$
$D_s^+ \rightarrow \tau^+ \nu_\tau$	$(6.6 \pm 0.6) \times 10^{-2}$
$\tau^- \rightarrow \mu^- \mu^- \mu^+$	$< 3.2 \times 10^{-8}$
$\tau^- \rightarrow \mu^- \gamma$	$< 4.5 \times 10^{-8}$
$\tau^- \rightarrow \mu^- \eta$	$< 6.5 \times 10^{-8}$
$\tau^- \rightarrow \mu^- \eta'$	$< 1.3 \times 10^{-7}$

Table 1: Present status of the observed branching ratios of $D_s^+ \rightarrow \ell^+ \nu$ ($\ell = \mu, \tau$) and the experimental upper limits on different LFV τ decays at 90% C.L. We have quoted numbers cited in Particle Data Group [9], although slightly stronger constraints in some channels exist [16]. The expected reach at the SuperB factory with 75 ab^{-1} data for $\tau^- \rightarrow \mu^- \mu^- \mu^+$ and $\tau^- \rightarrow \mu^- \eta$ channels are $2 \cdot 10^{-10}$ and $4 \cdot 10^{-10}$, respectively – see the SuperB conceptual design report [17].

Existing limits on λ' : We reiterate that all our processes are driven by λ'_{223} and λ'_{323} . The existing limits on them depend on $m_{\tilde{b}_R}$. As mentioned before, throughout our analysis we have assumed a common sparticle mass of 300 GeV. The best upper limit on λ'_{223} comes from $R_{D^0} \equiv \frac{\text{Br}(D^0 \rightarrow K^- \mu^+ \nu_\mu)}{\text{Br}(D^0 \rightarrow K^- e^+ \nu_e)}$, and the limit is 0.3 at 90% C.L. [3, 18]¹. On the other hand, the best upper limit on λ'_{323} arises from $R_{D_s}(\tau\mu) \equiv \frac{\text{Br}(D_s^+ \rightarrow \tau^+ \nu_\tau)}{\text{Br}(D_s^+ \rightarrow \mu^+ \nu_\mu)}$, the limit being 0.9 at 90% C.L. [3].

¹It is interesting to observe that the 2σ upper limit $|\lambda'_{22k}| < 0.16$ obtained in [18] with $R_{D^0} = 0.84 \pm 0.12$ is not much different from the latest update $|\lambda'_{22k}| < 0.1$ at 2σ for $\tilde{m} = 100 \text{ GeV}$ using $R_{D^0} = 0.92 \pm 0.04$ [3]. In spite of a significant reduction of the error on R_{D^0} (over a period of 14 years), the 2σ upper limit on $|\lambda'_{22k}|$ remained more or less the same because the central value gradually moved towards unity.

Our parameters: Recall that maximal mixing between ν_μ and ν_τ motivated us to assume $\lambda'_{223} = \lambda'_{323} = \lambda'$. For showing numerical correlations through different plots, we scan λ' in the range $[0 - 0.7]$, but keep \tilde{m} fixed at 300 GeV. Also, the band width in each plot is a consequence of varying f_{D_s} by 2σ around its central value, i.e. in the range $[235 - 247]$ MeV. As we go from left to right in each band the value of f_{D_s} increases. The minimum values of λ' consistent with 2σ lower limits of $\text{Br}(D_s \rightarrow \mu\nu)$ and $\text{Br}(D_s \rightarrow \tau\nu)$ are 0.3 and 0.4, respectively, which correspond to (the 2σ upper limit of) $f_{D_s} = 247$ MeV.

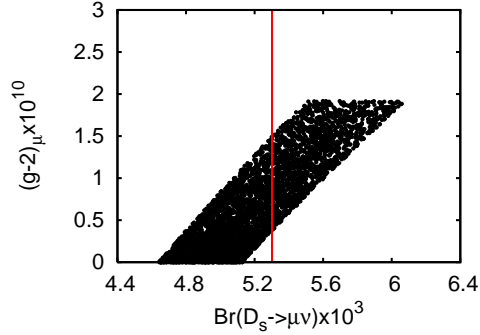


Figure 6: Correlation between the $\text{Br}(D_s \rightarrow \mu\nu)$ and the muon anomalous magnetic moment. The λ'_{223} -induced contribution to the latter is well below the current experimental sensitivity – see Eq. (4). The vertical line indicates 2σ lower limit of the branching ratio – see Table 1.

Contribution to $(g - 2)_\mu$: Following Eq. (5), we obtain

$$a_\mu^{\lambda'} \simeq 1.9 \cdot 10^{-10} \left(\frac{\lambda'}{0.7} \right)^2 \left(\frac{300}{\tilde{m} \text{ (in GeV)}} \right)^2. \quad (26)$$

In Fig. 6, we have plotted the correlation between contribution to $(g - 2)_\mu$ along one axis and the branching ratio of $D_s \rightarrow \mu\nu$ along the other. We note here that the R -parity conserving contribution to $(g - 2)_\mu$ can be sizable too for large $\tan\beta$. In fact, an approximate expression for $\tan\beta \gg 1$ can be found in [19] as

$$a_\mu^{\text{MSSM}} \simeq 1.7 \cdot 10^{-10} \tan\beta \left(\frac{300}{\tilde{m} \text{ (in GeV)}} \right)^2. \quad (27)$$

LFV τ decays: The approximate (yet, to a very good accuracy) expressions of the LFV form-factors with their explicit dependence on λ' and \tilde{m} (the other parameters are all known) are as follows:

$$\begin{aligned} A_L &\simeq -2.9 \cdot 10^{-7} \text{ GeV}^{-2} \left(\frac{\lambda'}{0.7} \right)^2 \left(\frac{300}{\tilde{m} \text{ (in GeV)}} \right)^2, & A_R &\simeq 8.6 \cdot 10^{-9} \text{ GeV}^{-2} \left(\frac{\lambda'}{0.7} \right)^2 \left(\frac{300}{\tilde{m} \text{ (in GeV)}} \right)^2, \\ B_L &\simeq 2.8 \cdot 10^{-7} \text{ GeV}^{-2} \left(\frac{\lambda'}{0.7} \right)^4 \left(\frac{300}{\tilde{m} \text{ (in GeV)}} \right)^2, & F_{LL} &\simeq 1.3 \cdot 10^{-9} \text{ GeV}^{-2} \left(\frac{\lambda'}{0.7} \right)^2 \left(\frac{300}{\tilde{m} \text{ (in GeV)}} \right)^2, \\ F_{LR} &\simeq -1.1 \cdot 10^{-9} \text{ GeV}^{-2} \left(\frac{\lambda'}{0.7} \right)^2 \left(\frac{300}{\tilde{m} \text{ (in GeV)}} \right)^2, & D_L &\simeq 5.1 \cdot 10^{-8} \text{ GeV}^{-2} \left(\frac{\lambda'}{0.7} \right)^4 \left(\frac{300}{\tilde{m} \text{ (in GeV)}} \right)^2. \end{aligned} \quad (28)$$

Since each box has four λ' -vertices, B_L and D_L have both quartic sensitivity to λ' , while the penguin form-factors have quadratic dependence on λ' . Using the expressions in Eq. (28), we calculate the branching ratios to a very good approximation as

$$\text{Br}(\tau \rightarrow \mu\mu\mu) \simeq 3.9 \cdot 10^{-7} \left[1.0 - 0.6 \left(\frac{\lambda'}{0.7} \right)^2 + 0.1 \left(\frac{\lambda'}{0.7} \right)^4 \right] \left(\frac{\lambda'}{0.7} \right)^4 \left(\frac{300}{\tilde{m} \text{ (in GeV)}} \right)^4; \quad (29)$$

$$\text{Br}(\tau \rightarrow \mu\gamma) \simeq 1.0 \cdot 10^{-6} \left(\frac{\lambda'}{0.7} \right)^4 \left(\frac{300}{\tilde{m} \text{ (in GeV)}} \right)^4; \quad (30)$$

$$\text{Br}(\tau \rightarrow \mu\eta) \simeq 3.4 \cdot 10^{-7} \left(\frac{\lambda'}{0.7}\right)^8 \left(\frac{300}{\tilde{m} \text{ (in GeV)}}\right)^4; \quad (31)$$

$$\text{Br}(\tau \rightarrow \mu\eta') \simeq 3.3 \cdot 10^{-7} \left(\frac{\lambda'}{0.7}\right)^8 \left(\frac{300}{\tilde{m} \text{ (in GeV)}}\right)^4. \quad (32)$$

In Eq. (29), the first term within the square bracket is the pure penguin contribution, the second term represents interference between penguin and box graphs, while the last term is the pure box contribution. As explained before, the λ' dependence is different for different terms. Also, by comparing Eq. (30) with Eq. (29), we observe that for the same choices of λ' and \tilde{m} the prediction of $\text{Br}(\tau \rightarrow \mu\gamma)$ is one order of magnitude enhanced compared to $\text{Br}(\tau \rightarrow \mu\mu\mu)$. This happens primarily because the latter is a 3-body decay which involves more suppression factors which cannot compensate the fact that $|A_R| \simeq |A_L|/33$. Figs. 7a and 7b capture the numerical correlations. We observe that the region allowed at 2σ by $D_s \rightarrow \tau\nu$ overshoots the 90% C.L. upper limit of the branching ratio of $\tau \rightarrow \mu\mu\mu$. Obviously, the same thing happens for $\tau \rightarrow \mu\gamma$. However, we should keep in mind that the branching ratio of $D_s \rightarrow \ell\nu$ ($\ell = \tau$ in the present context) has not only an experimental uncertainty, but also inherits a theoretical uncertainty from f_{D_s} . Even by *mild* stretching of one or both of these uncertainties beyond 2σ , it is possible to accommodate both $\tau \rightarrow \mu\mu\mu$ and $\tau \rightarrow \mu\gamma$.

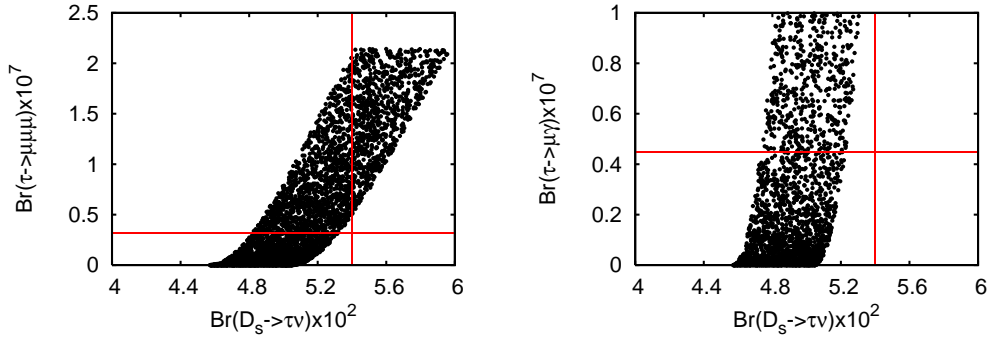


Figure 7: Correlations between (a) $\text{Br}(\tau \rightarrow \mu\mu\mu)$ and $\text{Br}(D_s \rightarrow \tau\nu)$ in the left panel, and (b) $\text{Br}(\tau \rightarrow \mu\gamma)$ and $\text{Br}(D_s \rightarrow \tau\nu)$ in the right panel. The vertical line in each plot corresponds to 2σ lower limit of the D_s branching ratio, while the horizontal lines are the 90% C.L. upper limits of the LFV τ decay branching ratios – see Table 1.

New Limit: The upper limit on $\tau \rightarrow \mu\gamma$ branching ratio (see Table 1) restricts $\lambda' < 0.3$. Our limit is stronger than before and, without any need of the assumption $\lambda'_{223} = \lambda'_{323}$, should be interpreted as

$$|\lambda'_{223} \lambda'_{323}| < 0.09 \text{ at } 90\% \text{ C.L.} \quad (33)$$

Since the D_s branching ratios require $\lambda' > (0.3 - 0.4)$ at 2σ (or 90% C.L.), to avoid conflict with Eq. (33) we need to stretch the present limits, as already mentioned. If we fix $\lambda' = 0.3$, the prediction for the branching ratio of $\tau \rightarrow \mu\mu\mu$ is $\sim 1.2 \cdot 10^{-8}$, which is roughly a factor of 3 below the current sensitivity, but still very much within the reach of the super B factory with 75 ab^{-1} projected luminosity. If, however, $\tau \rightarrow \mu\gamma$ remains elusive even at super B , then as per our prediction, $\tau \rightarrow \mu\mu\mu$ is not going to be observed either.

The branching ratio of $\tau \rightarrow \mu P$, expressed in Eq. (23), contains contributions from box (the D_L part) and penguin (the F_L part). The box contribution is significantly more dominant than the penguin. We display the approximate numerical values of the branching ratios for $P = \eta$ and η' in Eqs. (31) and (32), respectively. The dependences on λ' and \tilde{m} are similar as both processes involve similar box graphs. As expected, these modes are not as constraining as $\tau \rightarrow \mu\gamma$. If we put $\lambda' = 0.3$, the branching ratios for the η and η' modes are predicted to be around $4 \cdot 10^{-10}$, i.e. two orders of magnitude below the present sensitivity, but within the accuracy expected to be reached at the super B factory with 75 ab^{-1} luminosity. Again, a positive signal at Super B necessarily requires an observation of $\tau \rightarrow \mu\gamma$ at the current sensitivity. The numerical correlations of $\tau \rightarrow \mu\eta$ and $\tau \rightarrow \mu\eta'$ decay modes with the $D_s \rightarrow \tau\nu$ branching fraction have been plotted in Fig. 8.

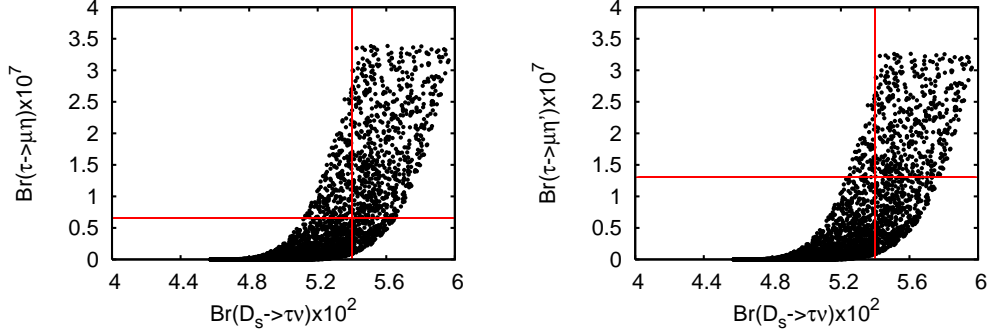


Figure 8: Exactly like in Fig. 7, except that the branching ratios of $\tau \rightarrow \mu\eta$ and $\tau \rightarrow \mu\eta'$ are plotted in (a) the left panel and (b) the right panel, respectively. The horizontal lines are the 90% C.L. upper limits on the branching ratios.

8 Comparison with previous works and conclusions

We divide this section in three parts: (i) we briefly mention about the existing studies on R -parity conserving supersymmetric contribution to LFV τ decays, (ii) remark on the previous works on R -parity violating contributions to lepton flavor violation, and finally (iii) highlight the new things that we have done in this work.

(i) LFV decays have been analyzed in supersymmetric scenarios with conserved R -parity but with different sets of supersymmetry breaking parameters. In a class of scenarios where minimal supersymmetry is augmented by three right-handed neutrino superfields for generating neutrino masses *via* see-saw mechanism, it has been shown [14, 20] that large neutrino Yukawa couplings induce large flavor violation in the slepton sector which is ultimately transmitted to the LFV observables. The general conclusion is that light supersymmetry ($m_0, M_{1/2} < 250$ GeV) is disfavored. Large LFV branching ratios (with large $\tan\beta \sim 50$) can be obtained when light neutrino masses are hierarchical. In general, $\tau \rightarrow \mu\gamma$ is the most sensitive LFV channel, but to explore the Higgs sector $\tau \rightarrow \mu\eta$ and $\tau \rightarrow \mu\eta'$ channels are more effective. It has been shown that in a general *unconstrained* minimal supersymmetric framework [21], for low $\tan\beta \sim 3$, the branching ratio in the $\tau \rightarrow \mu\mu\mu$ channel is $\mathcal{O}(10^{-9})$ and in the $\tau \rightarrow \mu\eta(\eta')$ channel less than 10^{-10} . On the other hand, for large $\tan\beta \sim 50$ and for small pseudo-scalar mass (m_A), the Higgs mediated contributions are extremely dominant. In the latter case, indeed with strong fine-tuning of parameters, $\text{Br}(\tau \rightarrow \mu\mu\mu)$ is enhanced to $\mathcal{O}(10^{-7})$ and $\text{Br}(\tau \rightarrow \mu\eta)$ to even larger values. In supersymmetric models embedded in minimal SO(10) group [22], the LFV branching ratios are, however, several orders of magnitude below the present experimental sensitivities.

(ii) RPV induced LFV processes have been studied in the past in different contexts [23]. Except $\ell_i \rightarrow \ell_j\gamma$, all other LFV processes considered there proceed at *tree level* with appropriately chosen RPV couplings. The choices of such couplings are, in general, different in different processes. Their primary intentions were to put upper limits on different single and product couplings by confronting LFV observables with experimental results.

(iii) *What are the new things that we have done in this paper?* We made an economical choice of RPV couplings (λ'_{223} and λ'_{323} only), motivated *primarily* by their ability to explain the large $D_s \rightarrow \ell\nu$ ($\ell = \mu, \tau$) branching ratios. We set these two couplings equal, a choice inspired by maximal ν_μ - ν_τ mixing. We have kept the sparticle mass fixed at 300 GeV. Explanation of $D_s \rightarrow \mu\nu(\tau\nu)$ branching ratios require $\lambda' > 0.3(0.4)$ at 90% C.L. On the other hand, $\tau \rightarrow \mu\gamma$ with an upper limit of $4.5 \cdot 10^{-8}$ on its branching ratio at 90% C.L. offers the most sensitive LFV probe of the RPV dynamics, and sets an *improved upper limit* $\lambda' < 0.3$ at 90% C.L. Enhanced theoretical and experimental accuracies in the $D_s \rightarrow \ell\nu$ channels might eventually release the tension between the apparently conflicting requirements. Putting $\lambda' = 0.3$, we obtain $\text{Br}(\tau \rightarrow \mu\mu\mu) \sim 1.2 \cdot 10^{-8}$, and $\text{Br}(\tau \rightarrow \mu\mu\mu) \div \text{Br}(\tau \rightarrow \mu\eta/\eta') \simeq 30$. The correlation plots capture the underlying dynamics. To sum up, instead of considering just one experimental observation at a time, be it an anomaly or an excess *vis-à-vis* the SM expectation, providing a *raison d'être* for one set of new interactions, we have studied the possibility of correlated enhancements in a variety of LFV channels using just two RPV couplings. We demonstrated our results through ‘observable versus observable’ plots.

Acknowledgments: GB thanks the CERN Theory Division for hospitality and acknowledges a partial support through the project No. 2007/37/9/BRNS of BRNS (DAE), India. SN's work is supported by a European Community's Marie-Curie Research Training Network under contract MRTN-CT-2006-035505 'Tools and Precision Calculations for Physics Discoveries at Colliders'.

References

- [1] G. R. Farrar and P. Fayet, Phys. Lett. B **76** (1978) 575; S. Weinberg, Phys. Rev. D **26** (1982) 287; N. Sakai and T. Yanagida, Nucl. Phys. B **197** (1982) 533; C. S. Aulakh and R. N. Mohapatra, Phys. Lett. B **119** (1982) 136.
- [2] For reviews see, G. Bhattacharyya, Nucl. Phys. Proc. Suppl. **52A** (1997) 83 [arXiv:hep-ph/9608415]; G. Bhattacharyya, arXiv:hep-ph/9709395; H. K. Dreiner, arXiv:hep-ph/9707435; M. Chemtob, Prog. Part. Nucl. Phys. **54** (2005) 71 [arXiv:hep-ph/0406029]; R. Barbier *et al.*, Phys. Rept. **420** (2005) 1 [arXiv:hep-ph/0406039].
- [3] For a very recent update on single RPV couplings, see Y. Kao and T. Takeuchi, arXiv:0910.4980 [hep-ph].
- [4] A. Kundu and S. Nandi, Phys. Rev. D **78** (2008) 015009 [arXiv:0803.1898 [hep-ph]]. A possible contribution from λ' product couplings has also been mentioned in A. G. Akeroyd and S. Recksiegel, Phys. Lett. B **554** (2003) 38 [arXiv:hep-ph/0210376].
- [5] S. Nandi and J. P. Saha, Phys. Rev. D **74** (2006) 095007 [arXiv:hep-ph/0608341].
- [6] G. Bhattacharyya, H. V. Klapdor-Kleingrothaus and H. Pas, Phys. Lett. B **463** (1999) 77 [arXiv:hep-ph/9907432]; S. Rakshit, G. Bhattacharyya and A. Raychaudhuri, Phys. Rev. D **59** (1999) 091701 [arXiv:hep-ph/9811500]. A. Abada, G. Bhattacharyya and M. Losada, Phys. Rev. D **66** (2002) 071701 [arXiv:hep-ph/0208009]. This is only a partial list. See [2] for other references on neutrino mass generation by RPV couplings.
- [7] P. Dey, A. Kundu, B. Mukhopadhyaya and S. Nandi, JHEP **0812** (2008) 100 [arXiv:0808.1523 [hep-ph]].
- [8] T. Onogi, arXiv:0906.5194 [hep-ph].
- [9] C. Amsler *et al.* [Particle Data Group], Phys. Lett. B **667** (2008) 1, and <http://pdg.lbl.gov> for 2009 partial update.
- [10] B. I. Eisenstein *et al.* [CLEO Collaboration], Phys. Rev. D **78** (2008) 052003 [arXiv:0806.2112 [hep-ex]]. An updated CLEO result can be found in arXiv:0910.3602. We thank Sheldon Stone for pointing this out to us.
- [11] K. Abe *et al.* [Belle Collaboration], Phys. Rev. Lett. **100** (2008) 241801 [arXiv:0709.1340 [hep-ex]].
- [12] B. A. Dobrescu and A. S. Kronfeld, Phys. Rev. Lett. **100** (2008) 241802 [arXiv:0803.0512 [hep-ph]]; R. Benbrik and C. H. Chen, Phys. Lett. B **672** (2009) 172 [arXiv:0807.2373 [hep-ph]]; I. Dorsner, S. Fajfer, J. F. Kamenik and N. Kosnik, arXiv:0906.5585 [hep-ph].
- [13] F. Jegerlehner and A. Nyffeler, Phys. Rept. **477** (2009) 1 [arXiv:0902.3360 [hep-ph]]. For a recent update, see J. Prades, arXiv:0909.2546 [hep-ph].
- [14] E. Arganda and M. J. Herrero, Phys. Rev. D **73** (2006) 055003 [arXiv:hep-ph/0510405]; J. Hisano, T. Moroi, K. Tobe and M. Yamaguchi, Phys. Rev. D **53** (1996) 2442 [arXiv:hep-ph/9510309].
- [15] T. Feldmann and P. Kroll, Eur. Phys. J. C **5** (1998) 327 [arXiv:hep-ph/9711231].
- [16] S. Banerjee, Nucl. Phys. Proc. Suppl. **169** (2007) 199 [arXiv:hep-ex/0702017].
- [17] M. Bona *et al.*, "SuperB: A High-Luminosity Asymmetric e^+e^- Super Flavor Factory. Conceptual Design Report," arXiv:0709.0451 [hep-ex].
- [18] G. Bhattacharyya and D. Choudhury, Mod. Phys. Lett. A **10** (1995) 1699 [arXiv:hep-ph/9503263].

- [19] M. S. Carena, G. F. Giudice and C. E. M. Wagner, *Phys. Lett. B* **390** (1997) 234 [arXiv:hep-ph/9610233]. See also (a partial list), T. Moroi, *Phys. Rev. D* **53** (1996) 6565 [Erratum-ibid. *D* **56** (1997) 4424] [arXiv:hep-ph/9512396]; U. Chattopadhyay and P. Nath, *Phys. Rev. D* **53** (1996) 1648 [arXiv:hep-ph/9507386]; R. Barbieri and L. Maiani, *Phys. Lett. B* **117** (1982) 203.
- [20] E. Arganda, M. J. Herrero and J. Portoles, *JHEP* **0806** (2008) 079 [arXiv:0803.2039 [hep-ph]]; K. S. Babu and C. Kolda, *Phys. Rev. Lett.* **89** (2002) 241802 [arXiv:hep-ph/0206310].
- [21] A. Brignole and A. Rossi, *Nucl. Phys. B* **701** (2004) 3 [arXiv:hep-ph/0404211].
- [22] T. Fukuyama, A. Ilakovac and T. Kikuchi, *Eur. Phys. J. C* **56** (2008) 125 [arXiv:hep-ph/0506295];
- [23] H. K. Dreiner, M. Kramer and B. O'Leary, *Phys. Rev. D* **75** (2007) 114016 [arXiv:hep-ph/0612278]; J. Cao, L. Wu and J. M. Yang, arXiv:0908.4556 [hep-ph]; W. j. Li, Y. d. Yang and X. d. Zhang, *Phys. Rev. D* **73** (2006) 073005 [arXiv:hep-ph/0511273]; A. Gemintern, S. Bar-Shalom, G. Eilam and F. Krauss, *Phys. Rev. D* **67** (2003) 115012 [arXiv:hep-ph/0302186]; K. m. Cheung and O. C. W. Kong, *Phys. Rev. D* **64** (2001) 095007 [arXiv:hep-ph/0101347]; A. de Gouvea, S. Lola and K. Tobe, *Phys. Rev. D* **63** (2001) 035004 [arXiv:hep-ph/0008085]; J. E. Kim, P. Ko and D. G. Lee, *Phys. Rev. D* **56** (1997) 100 [arXiv:hep-ph/9701381]; D. Choudhury and P. Roy, *Phys. Lett. B* **378** (1996) 153 [arXiv:hep-ph/9603363].